Non-hydrostatic depth-integrated models for dam break flows through rigid-emergent vegetation

Adel A. Mahmoud[1,2], *Bobby Minola* Ginting[1,3], and *Tatsuhiko* Uchida[1*]

[1]Graduate School of Advanced Science and Engineering, Hiroshima University, Higashi-Hiroshima City, Hiroshima 739-8527, Japan
[2]Sohag Faculty of Engineering, Sohag University, Sohag 82524, Egypt
[3]Department of Civil Engineering, Parahyangan Catholic University, Jl. Ciumbuleuit No. 94, Bandung, West Java 40141, Indonesia

Abstract. Dam failures can trigger catastrophic downstream flooding, threatening lives, and infrastructure. Vegetation acts like a natural dam break flow buffer, dissipating energy, reducing wave height and celerity. This highlights importance of vegetation in flood mitigation strategies. Few existing numerical models consider how vegetation affects dam breaks. This is because it is difficult to calculate vegetation drag force in unsteady rapidly varied flows. This study addresses this gap by developing a non-hydrostatic depth-integrated model to simulate the effect of rigid emergent vegetation on dam break flows under various flow conditions. The model was validated with experimental data. Vegetation was simulated with wooden cylinders with different coverage areas and densities within a straight channel. Three dam break scenarios were investigated in the experiment using different Froude numbers to represent diverse flow regimes. The non-hydrostatic depth-integrated model of the General Bottom Velocity method (GBVC4-DWL) was developed to incorporate the vegetation effect through the drag force equation for non-uniform open channel flows. The results show that rigid emergent vegetation significantly reduces wave celerity and height, particularly downstream, demonstrating its importance in flood mitigation. The numerical model accurately predicted wave behaviour outside the vegetation zone but have difficulties within it, highlighting the need for the model to be improved to capture complex vegetation-flow interactions.

1 Introduction

Dam failures pose a significant threat to downstream communities due to sudden water releases that can cause property damage and loss of life (e.g., Banqiao Dam failure, China, 1975). This has driven research efforts to understand dam break flows. Because direct field measurement of dam break flows is difficult, researchers have relied on both experimental and numerical models. Previous experimental studies have investigated the influence of various parameters on dam break flows [1, 2]. Numerical models offer an alternative,

*Corresponding author: utida@hiroshima-u.ac.jp

allowing researchers to explore different scenarios. The numerical models include one-dimensional 1D, two-dimensional 2D, three-dimensional 3D, and Quasi-3D models [3–5]. Rigid vegetation plays a crucial role in dissipating flow energy, reducing both water depth and velocity [6], highlighting its potential as a natural flood mitigation strategy. Despite its important impact, few studies have explored effect of vegetation on dam break flows. Zhang et al. [7] and He et al. [8] numerically investigated the effect of vegetation that partially covered the channel on dam break flow. Initially validated in scenarios excluding vegetation, their numerical models successfully matched experimental data. However, their validation did not extend to cases involving vegetation effects, revealing a limitation in evaluating the models' accuracy under such conditions. As reviewed above, the authors found that few studies investigated interaction among dam break flow and vegetation on movable bed.

This study introduces a numerical model to analyse the effect of vegetation on dam break flows. It utilizes a non-hydrostatic depth-integrated model of the General Bottom Velocity method coupled with dynamic rough wall law (GBVC4-DWL) [9], incorporating vegetation effects through a drag force equation [10]. The model was validated against experimental results with different initial conditions and vegetation characteristics which allows the model to be applicable to a wide range of real-world dam break flow scenarios.

2 Experimental Setup

Figure 1 illustrates the flume setup and vegetation characteristics. The flume channel was straight and horizontal, with dimensions of 16.20 m length, 0.40 m width, and 0.40 m depth. The channel walls and bottom were made of concrete with a Manning roughness coefficient of n = 0.013 $m^{1/3}/s$. The flume had solid walls at both the upstream and downstream ends. The reservoir, located at the upstream end, occupied 2.0 m of the flume length. A movable steel gate with a thickness of 4 mm was installed at the reservoir's end. To initiate sudden dam break flow, the gate was manually removed. Rigid emergent vegetation was simulated using wooden cylinders, each with a diameter of 1.0 cm. These cylinders were installed in a staggered arrangement within the channel.

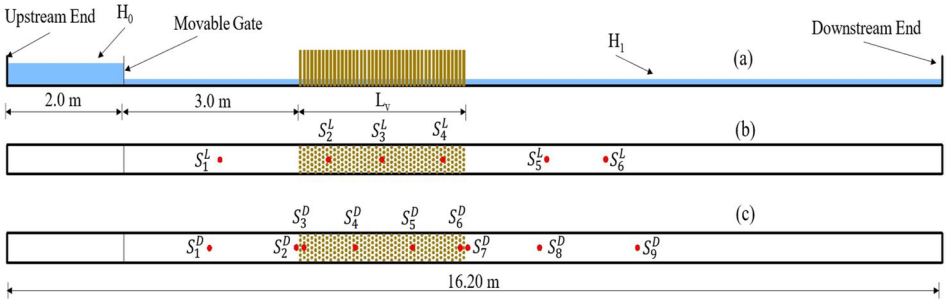

Fig. 1. Flume setup and vegetation characteristics (a) side view (b) plan view shows measurement sections for vegetation length cases (c) plan view shows measurement sections for vegetation density cases.

The experiment explored different flow scenarios by varying the water depths in the reservoir (H_0) and the downstream channel (H_1) behind the gate. Two reservoir depths were used in combination with three different static tailwater depths. These depths were adjusted using two gauges positioned strategically: one near the downstream end of the flume and another within the reservoir itself. These depths created three distinct flow scenarios represented by three different Froude number values resulting immediately after dam collapse, these values classified Froude number to High (F_r=3.98, Case*H), Middle (F_r=1.53,

Case*M), and Low Froude number (F_r=1.32, Case*L). Wave height variations over time were measured using a servo-type wave height meter (KENEK). The movable gate-opening time was determined using a digital camera positioned at the upstream end and a wave gauge just upstream of the gate.

Four different vegetation field lengths (L_v) with a constant volume density (λ=0.067) were investigated for Case L*1-4. Figure 1(b) illustrates the measurement sections for these cases.

Vegetation density was varied three times while maintaining a constant vegetation field length (L_v = 3.0 m) for Case D*1-3. To gain more insight into wave propagation and validate the numerical model, the measurement sections were expanded for these density cases (see Figure 1(c)). Table 1 summarizes the initial conditions for all experiments.

Table 1. Experimental initial conditions.

Case	**LH 1**	**LH 2**	**LH 3**	**LH 4**	**LM 1**	**LM 2**	**LM 3**	**LM 4**	**LL 1**	**LL 2**	**LL 3**	**LL 4**
Veg. field length L_v (m)	0.60	1.60	3.0	5.0	0.60	1.60	3.0	5.0	0.6	1.6	3.0	5.0
Veg. volume density λ	0.067											
Case	**DH1**	**DH2**	**DH3**	**DM1**	**DM2**	**DM3**	**DL1**	**DL2**	**DL3**			
Veg. volume density λ	0.125	0.062	0.031	0.125	0.062	0.031	0.125	0.062	0.031			
Veg. field length L_v (m)	3.0											
H_0 (m)	0.30			0.285								
H_1 (m)	0.02			0.107			0.147					
Froude number F_r	High (F_r=3.98)			Middle (F_r=1.53)			Low (F_r=1.32)					

Table 2 details the locations of the measurement sections along the flume channel. Distances are measured relative to the upstream end. The symbol S_1^L refers to section number 1 for the vegetation length cases, while the symbol S_1^D refers to section number 1 in the vegetation density cases.

Table 2. Details the locations of the measurement sections along the flume channel.

Section	$\mathbf{S_1^D}$	$\mathbf{S_2^D}$	$\mathbf{S_3^D}$	$\mathbf{S_4^D}$	$\mathbf{S_5^D}$	$\mathbf{S_6^D}$	$\mathbf{S_7^D}$	$\mathbf{S_8^D}$	$\mathbf{S_9^D}$
Distance (m)	3.50	4.97	5.03	6.0	7.0	7.96	8.03	9.50	11.0
Section	S_1^L	S_2^L	S_3^L	S_4^L	S_5^L	S_6^L			
Distance (m)	3.57	5.53	6.53	7.60	9.55	10.56			

3 Numerical models

The research methodology in this study is built upon the General Bottom Velocity Method combined with the Dynamic Rough Wall Law (GBVC4-DWL) as outlined by Uchida et al.[9]. This methodology incorporates the interaction between flow and vegetation by integrating a non-equilibrium open channel drag force equation [10]. While detailed mathematical formulations are provided in Uchida et al.[9], we highlight the unique approach used here, which includes additional terms to account for the drag force exerted on vegetation in the depth-integrated horizontal momentum equations (Equation (1)), the depth-integrated horizontal vorticity equations (Equation (2)), and the horizontal momentum equations on the water surface (Equation (3)) with considering a channel with uniform width.

$$\frac{\partial Uh}{\partial t}+\frac{\partial U^2h}{\partial x}-w_{\sigma b}u_b=-gh\frac{\partial z_s}{\partial x}-\frac{\tau_{bx}}{\rho}+\frac{\partial hT_{xx}}{\rho\partial x}-\left(\frac{\partial h\overline{P_d}}{\rho\partial x}+\frac{p_{db}}{\rho}\frac{\partial z_b}{\partial x}\right)-hF_x \quad (1)$$

$$\frac{\partial \Omega_y h}{\partial t} = R_{\sigma y} + P_{\omega y} + \frac{\partial h D_{\omega xx}}{\partial x} + w_{\sigma b}\omega_{by} - (f_{sx} - f_{bx}) \quad (2)$$

$$\frac{\partial u_s}{\partial t} + u_s \frac{\partial u_s}{\partial x} = -g\frac{\partial z_s}{\partial x} + P_{sx} - f_{sx} \quad (3)$$

For a detailed explanation of the variables employed in the equations, please refer to Uchida et al. [9]. The terms F_x, f_{sx}, and f_{bx} represent the drag force exerted by vegetation on the depth-averaged component, water surface, and channel bottom, respectively. The drag force Equation (4) for F_x encompasses components related to water surface variation and pressure gradient [10], calculated as:

$$F_x = Nd\left(\frac{C_D U^2}{2} - gkd\frac{U}{|U|}\frac{\partial h}{\partial x}\right)\frac{U}{|U|} \quad (4)$$

Here, N denotes the number of vegetation per meter square, d is the vegetation diameter. While the drag force term F_x considers the depth-averaged velocity U, the others, i.e., f_{sx}, and f_{bx} depend on the surface (u_s) and bottom (u_b) velocities, respectively. k is a coefficient to represent wake length behind the cylinder and C_D is the drag coefficient determined by the base component of drag force and Froude number F_r as in Equation (5):

$$\frac{C_D}{C_{D0}} = 1 + \frac{\beta_{cp}}{2} C_{C0} {F_r}^2 \quad (5)$$

where C_{D0} represents the drag coefficient under conditions of free stream flows where the Froude number approaches zero [10], and β_{cp}signifies the coefficient associated with the pressure coefficient distribution around a cylinder, in the current study, $\beta_{cp} = -0.4$.

The values of C_{D0} and k were derived from primary experiments under the steady state condition for each vegetation density to minimize the root mean square error (RMSE) between measured water depths and those calculated using depth profile equation for a flow incorporating drag force equation (Equation 4). Table 3 provides a detailed illustration of the values of C_{D0} and k corresponding to each density. With increasing vegetation density, the drag coefficient C_{D0} increases while the wake length coefficient k decreases.

Table 3. Values of C_{D0} and k corresponding to vegetation densities.

Veg. volume density λ	0.125	0.062	0.067	0.031
$\boldsymbol{C_{D0}}$	1.10	1.25	1.30	1.35
$\boldsymbol{k}$	8.60	4.20	5.0	2.60

4 Results and discussions

In this section, to discuss the effects of the vegetation, the channel is divided into three distinct regions: the upstream, inside, and downstream vegetation regions. While it is not feasible to include results for all measurement cases in every region, a subset of these cases will be presented, with the understanding that the unshown cases exhibit similar trends.

Figure 2 illustrates the temporal variation of wave height upstream of the vegetation at section number one (S_1) for High F_r conditions. As demonstrated in this figure, the GBVC-DWL model can accurately capture the propagation of the incident wave, as evidenced by the matching between the experimental and numerical results in terms of wave height and wave arrival time. While the model tends to underestimate the first peak of the incident wave, the discrepancies observed in the tail of the first wave for some cases were attributed to experimental uncertainties. Despite the model's success in capturing the incident wave propagation, it failed to accurately capture the propagation of the reflected wave from the vegetation to the upstream direction. This failure is manifested in the discrepancies observed between the experimental and numerical results, particularly in terms of arrival time and

wave height. The reflected wave is known to be affected by the frontal area of the vegetation [11], and consequently, the discrepancies in its height and arrival time differ with changing vegetation density, as shown in Figure 2. So, to improve the model's capability in accurately simulating the reflected wave behavior, it is necessary to refine the drag force equation that accounts for the interaction between the waves and the vegetation field.

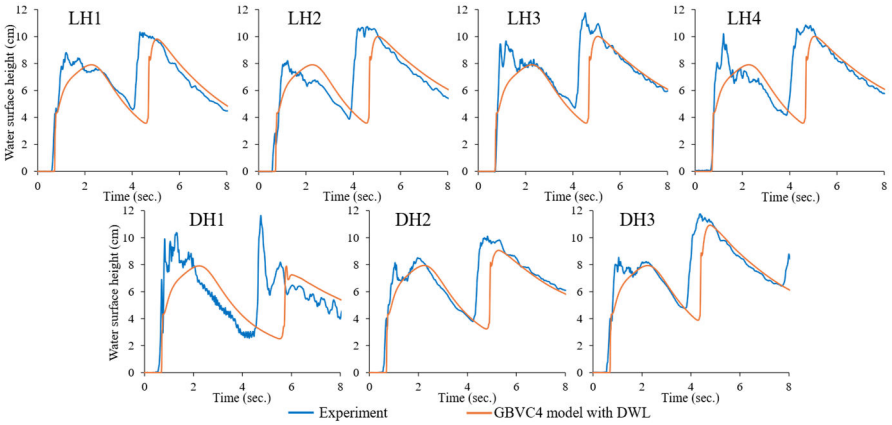

Fig. 2. Temporal variation of water surface height at S_1 for High F_r conditions.

For model validation within the vegetated zone, Figure 3 presents a comparison of the model's outputs for cases LM4 and DM3 with the corresponding experimental results for Middle F_r conditions. The model accurately predicts water surface height, yet it struggles to forecast wave celerity. This discrepancy is evident in the difference in wave arrival time between the experimental and model data, with the difference amplifying as the wave travels downstream. The disparity in wave arrival time between model and experiments decreases with reducing vegetation resistance, signified by lower vegetation density or shorter field length (not mentioned in Figure (3)). A similar issue was noted in a two-dimensional analysis method by KOBAYASHI and UCHID [12], but it remains unclear whether the discrepancy stems from the flow model or the hydrodynamic force model. This unresolved matter poses a future challenge that warrants attention, although it falls outside the scope of this study.

In the last region downstream of the vegetation, Figure 4 presents the results for both experiments and the numerical model under Low F_r conditions. As illustrated in the figure, the model accurately predicted wave propagation, including wave celerity and height, with a high degree of accuracy. The model's prediction of wave celerity is evident in the constant difference in wave arrival time between the experiment and the model as the wave propagates downstream. It should be noted that this difference in wave arrival time between the experiment and the model occurs specifically when the wave passes through the vegetation region itself. In the further downstream section, the wave height increased due to fluctuations observed under these Low F_r conditions. It is known that the dam break waves can be classified into breaking, undular with some breaking and pure undular waves according to Froude number values [13]

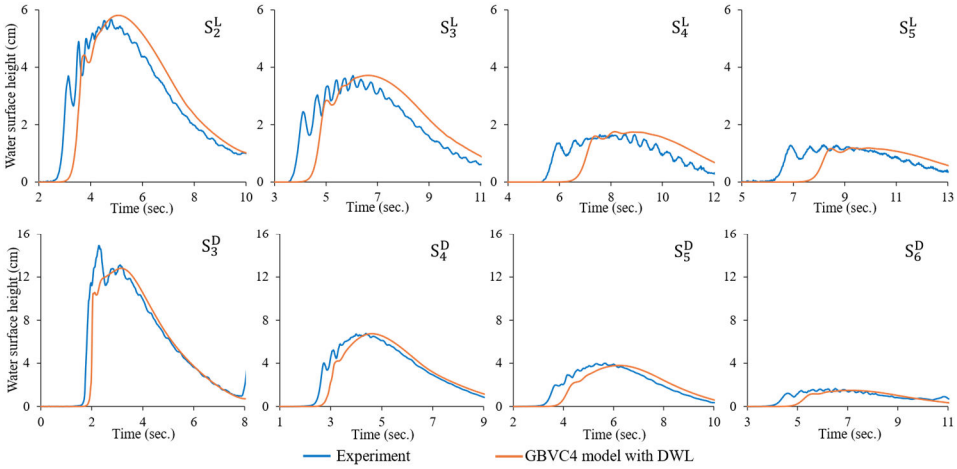

Fig. 3. Temporal variation of water surface height inside the vegetation field for LM4 case (upper figures) and DM3 case (lower figures) for Middle F_r conditions.

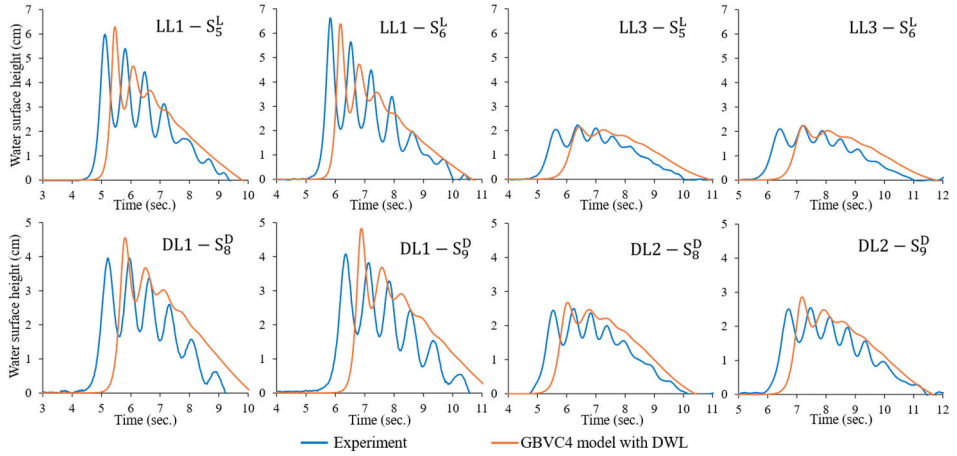

Fig. 4. Temporal variation of water surface height downstream of vegetation field under Low F_r conditions.

The model successfully captured this transition from breaking bore to undular bore with soliton fission for Low Froude number conditions, although the model overestimate the wave attenuation. Moreover, the model accurately simulated the impact of increasing vegetation density and vegetation field length, resulting in the damping of wave height and a decrease in wave celerity, evidenced by increasing in wave arrival time.

5 Conclusion

The conclusions drawn from the results of this study can be summarized as follows : The current study demonstrates proficiency of the model in simulating incident wave propagation but encounters difficulties with the reflected wave from vegetation. While the model effectively predicts water surface elevation within the vegetation zone, it struggles to accurately forecast wave celerity, particularly as vegetation resistance increases. Despite these challenges, the model performs well in capturing wave propagation characteristics downstream of the vegetation. The shortcomings of the model inside vegetation field

highlight the need for further refinement of the drag force equation incorporating in the current model.

References

1. W. Liu, B. Wang, Y. Guo, J. Zhang, Y. Chen, Experimental investigation on the effects of bed slope and tailwater on dam-break flows. J. Hydrol. **590**, 125256 (2020). https://doi.org/10.1016/j.jhydrol.2020.125256
2. H. Ozmen-Cagatay, E. Turhan, S. Kocaman, An experimental investigation of dam-break induced flood waves for different density fluids. Ocean Eng. **243**, 110227 (2022). https://doi.org/10.1016/j.oceaneng.2021.110227
3. M. Zhang, Y. Xu, Z. Hao, Y. Qiao, Integrating 1D and 2D hydrodynamic, sediment transport model for dam-break flow using finite volume method. Sci. China Phys. Mech. Astron. **57**, 774–783 (2014). https://doi.org/10.1007/s11433-013-5294-z
4. R. Marsooli, W. Wu, Three-Dimensional Numerical Modeling of Dam-Break Flows with Sediment Transport over Movable Beds. J. Hydraul. Eng. **141**, 04014066 (2015). https://doi.org/10.1061/(ASCE)HY.1943-7900.0000947
5. T. Uchida, S. Fukuoka, Quasi-3D two-phase model for dam-break flow over movable bed based on a non-hydrostatic depth-integrated model with a dynamic rough wall law. Adv. Water Resour. **129**, 311–327 (2019). https://doi.org/10.1016/j.advwatres.2017.09.020
6. S. Gong, J. Chen, C. Jiang, S. Xu, F. He, Z. Wu, Prediction of solitary wave attenuation by emergent vegetation using genetic programming and artificial neural networks. Ocean Eng. **234**, 109250 (2021). https://doi.org/10.1016/j.oceaneng.2021.109250
7. M. Zhang, Y. Xu, Y. Qiao, H. Jiang, Z. Zhang, G. Zhang, Numerical simulation of flow and bed morphology in the case of dam break floods with vegetation effect. J. Hydrodyn. **28**, 23–32 (2016). https://doi.org/10.1016/S1001-6058(16)60604-2
8. Z. He, T. Wu, H. Weng, P. Hu, G. Wu, Numerical simulation of dam-break flow and bed change considering the vegetation effects. International J. Sediment Res. **32**, 105–120 (2017). https://doi.org/10.1016/j.ijsrc.2015.04.004
9. T. Uchida, S. Fukuoka, A. (Thanos) N. Papanicolaou, A. G. Tsakiris, Nonhydrostatic Quasi-3D Model Coupled with the Dynamic Rough Wall Law for Simulating Flow over a Rough Bed with Submerged Boulders. J. Hydraul. Eng. **142**, 04016054 (2016). https://doi.org/10.1061/(ASCE)HY.1943-7900.0001198
10. T. Uchida, T. Ato, D. Kobayashi, M. F. Maghrebi, Y. Kawahara, Hydrodynamic forces on emergent cylinders in non-uniform flow. Environ. Fluid Mech. **22**, 1355–1379 (2022). https://doi.org/10.1007/s10652-022-09898-7
11. A. Hoque, S. Husrin, H. Oumeraci, Laboratory studies of wave attenuation by coastal forest under storm surge. Coast. Eng. J. **60**, 225–238 (2018). https://doi.org/10.1080/21664250.2018.1486268
12. D. Kobayashi, T. Uchida, Propagation characteristics of breaking bores through a permeable resistance and its numerical evaluation method. J. of JSCE **80**, 23–16081 (2024). https://doi.org/10.2208/jscejj.23-16081
13. D. Kobayashi, T. Uchida, Experimental and numerical investigation of breaking bores in straight and meandering channels with different Froude numbers. Coast. Eng. J. **64**, 442–457 (2022). https://doi.org/10.1080/21664250.2022.2118431